I-330

OSM-EIRENE modeling of neutral pressures in the Alcator C-Mod divertor

S. Lisgo[a]*, P. Börner[c], C. Boswell[b], D. Elder[a], B. LaBombard[b], B. Lipschultz[b], D. Reiter[c], P.C. Stangeby[a], J.L. Terry[b], S. Wiesen[c]

[a]*University of Toronto Institute for Aerospace Studies, Toronto, M3H 5T6, Canada.*

[b]*MIT Plasma Science and Fusion Center, Cambridge, MA 02139, USA*

[c]*IPP, Forschungszentrum Juelich GmbH, EURATOM Association,D-52425 Juelich, Germany*

The ITER divertor will be more collisional than divertors in existing tokamaks. The neutral modeling tools used for predictive ITER modeling need to be validated for similar divertor conditions in order to increase confidence in the results. The EIRENE neutral code has been applied to the Alcator C-Mod divertor, where collisional effects such as Lyman series photon trapping and neutral viscosity have been observed. The plasma solution used as input to EIRENE agrees well with the available diagnostic data for the divertor and was generated using an empirical Onion-Skin Method interpretive code that requires a large amount of experimental data as input. The calculated divertor pressure is 11±2 mTorr, a factor ~2 lower than the measured value of 25±2 mTorr. The neutral solution is sensitive to photon trapping, viscosity, elastic collisions between plasma ions and molecules, and leakage through the outer divertor substructure.

JNM keywords: Monte Carlo Modeling, Plasma Materials Interaction, Plasma Properties

PSI-16 keywords: Alcator C-Mod, Divertor Modelling, OSM, EIRENE, Neutrals

PACS: 52.55, 52.20.H, 52.65

[*]*Corresponding author address:* UTIAS, 4925 Dufferin St., Toronto, Ontario, Canada M3H 5T6

[*]*Corresponding author e-mail:* steven@starfire.utias.utoronto.ca

Presenting author address: UTIAS, 4925 Dufferin St., Toronto, Ontario, Canada M3H 5T6

Presenting author e-mail: steven@starfire.utias.utoronto.ca

1. Introduction

The ITER divertor will have shorter neutral mean free path lengths scaled to machine size than the current generation of tokamaks, resulting in more strongly coupled neutral, ion and photon populations; see table 1. It is well known that neutral dynamics are an important component of edge physics [4] and are central to several ITER-critical issues such as detachment, pumping, impurities, and (perhaps) access to H-mode. Also, the strong absorption of Lyman series photons by atoms can significantly affect ionisation profiles [5]. Sophisticated kinetic Monte-Carlo neutral codes such as EIRENE [6] and DEGAS [7] are available for investigating these neutral interactions, but are typically applied assuming free-molecular transport and optical transparency.

Alcator C-Mod [8] is a high magnetic field (up to 9 Tesla) divertor tokamak that currently represents the best opportunity to validate neutral codes for ITER-like divertor conditions, a requirement for increased confidence in predictive modeling studies for ITER. Measured neutral pressures in the C-Mod divertor approach 100 mTorr, indicating the presence of neutral viscosity [9], and there have also been observations of strong Lyman α (Ly_α) photon trapping [5]. However, two initial efforts to calculate the divertor neutral pressure with DEGAS gave results a factor ~10 lower than the measured value. The first attempt employed a rather simple plasma solution [10] as input to DEGAS and therefore a large discrepancy is not surprising, but the subsequent plasma solution was more detailed and was generally consistent with a significant amount of spectroscopic data [11]. It has been suggested that inaccuracies in the plasma solution contributed significantly to the pressure discrepancy [12].

The objectives of the present study are: (a) use interpretive methods and the large amount of experimental data available for the C-Mod divertor to produce a sufficiently

accurate and detailed description of the divertor plasma, and then (b) *quantitatively* assess the sensitivity of the neutral solution to the neutral physics in EIRENE. A more complete account of the results presented here can be found in reference 13.

2. Generation of the divertor plasma solution

EIRENE requires 2D distributions of the electron temperature, T_e, and plasma density, n_e, as input (assuming toroidal symmetry and $T_i = T_e$). The standard edge 2D fluid codes are most commonly used to specify the T_e and n_e profiles, but an interpretive method termed "empirical reconstruction" that relies extensively on experimental data is utilized in the present work. Discharge 990429019 at 950 ms is modeled, with $\overline{n}_e = 1.46\times10^{20}$ m^{-3}, deuterium majority, lower single-null, and B×∇B towards the divertor; the same shot that was used for the previous efforts to model the divertor pressure with DEGAS. A review of the diagnostic data indicates partial detachment in the inner divertor and outer PFZ, where $T_e \approx 1$ eV and $n_e \approx 10^{21}$ m^{-3} ; see section 2.2. Volume recombination is very sensitive to T_e and n_e for these plasma conditions [14] which suggests that the divertor neutral solution is strongly dependant on the T_e and n_e profiles input to EIRENE. The low T_e values also imply neutral ionization/dissociation mean free paths on the order of the geometric scale length, so that a detailed plasma solution is required for the entire divertor, not just near the gas box where the pressure measurement is made.

2.1 Empirical reconstruction of the detached plasma profiles

The plasma solution is generated by the OSM code which employs the Onion-Skin Method [15]. The boundary conditions are specified in the divertor, and the full 2D solution is

assembled from a series of nested 1D solutions for individual flux-tubes. $T_i = T_e$ is assumed and is a reasonable approximation given the short e-i equilibration times in the C-Mod divertor.

The interpretive method used to generate the detached plasma profiles is detailed elsewhere [13,16]. In brief, a simple parameterized model of detachment is used as a template for detached plasma profiles; the parameters are set from comparisons with experimental data. The validity of the resulting T_e, n_e distributions depends on the level of agreement with experiment and on having sufficient data available to constrain the solution.

The standard OSM 1D fluid model [16], based on conservation equations, is applied for the attached plasma in the outer SOL and upstream of the detached region in the inner SOL.

2.2 Comparison with the available experimental data for the divertor

Considerable experimental effort has been made to measure the plasma conditions in the C-Mod divertor; see figure 1.

The divertor pressure is measured at the bottom of a 1.26 m vertical access port which descends from the floor of the gas box (referred to here as "the plenum") located behind the outer target. The measured value, p_{div}^{expt}, is 25 ± 3 mTorr.

Langmuir probe arrays are embedded in the inner and outer target plates [17]. The probe T_e data for the inner divertor are shown in figure 2a, and the data points above the inner nose are much higher than T_e values estimated from Balmer line ratios; see figure 4a for $\theta <$ 161°. The difficulty interpreting the Langmuir probe characteristics is consistent with similar comparisons on other tokamaks [18], and Langmuir probe T_e data are generally considered unreliable below ~5 eV. Therefore, the model T_e boundary conditions for the inner divertor

are set based on agreement with spectroscopic data, although note that the probes below the inner nose are in reasonable agreement with the model. The I_{sat} measurements are applied as boundary conditions but there are no data for the inner PFZ and so nominal values are estimated; see figure 2b. Figure 2e shows substantial pressure loss between the inner target and the upstream reciprocating probe, consistent with detachment. Conversely, the outer SOL probe data shown in figures 2c-e are typical of attached conditions. The probe T_e values drop to ~1 eV in the outer PFZ, in agreement with the spectroscopic data; see figure 3a for θ = 260.5°. The apparent reliability of the outer divertor Langmuir probes for low T_e is unexplained at present.

The top- and side-view spectrometer and diode array data are compared with the model in figures 3 and 4, respectively. The temperature data, $T_{e,Saha}$, is calculated by fitting the measured emission ratios of the p = 6,7,8,9→2 Balmer lines to the Saha equation [2]. Stark broadening analysis [2] of these lines also gives an estimate of the electron density, $n_{e,Stark}$. These data are representative of (detached) plasma that is recombining in the volume since excitation of atoms by electron impact does not efficiently populate these higher Balmer lines. There is general agreement with the $T_{e,Saha}$ and $n_{e,Stark}$ data, although the model is just outside the stated uncertainty in some cases. The $T_{e,Saha}$ = 0.5 eV data point above the outer nose is due to light reflections [20], which are included in the simulation of the diagnostic. The high resolution diode arrays were equipped with a D_α filter and the model matches the shape of the measured profiles well but is higher in magnitude by a factor ~2.

The D_γ distribution from the inversion of the toroidally viewing camera is shown in figure 5a. The model result in figure 5b matches the distribution, but as with D_α, the calculated values are higher by a factor ~2. The discrepancy may be due to underestimates of the uncertainty in the experimental data or inaccuracies in the atomic physics. Modifying the plasma solution to reduce the line emissions produces clear disagreement with the $T_{e,Saha}$ and

$n_{e,Stark}$ data; the presented D_α and D_γ results give the best *overall* agreement with the full spectroscopic data set.

Comparison with the reciprocating probe data is beyond the scope of this monograph and is presented in reference 13.

2.3 Plasma solution

The plasma solution is plotted in figure 6. T_e in the PFZ is highest near the outer leg of the separatrix and decreases to ~0.5 eV in the lower divertor. The plasma density peaks at $\sim 10^{21}$ m^{-3} near the x-point and near the separatrix in the outer PFZ. Given the broad agreement with the experimental data, it is hypothesized that the plasma solution is sufficiently accurate for investigating neutral dynamics in the C-Mod divertor.

3. Neutral Modeling Results and Discussion

The divertor pressure calculated by EIRENE, p_{div}^{code}, is 17 ± 2 mTorr for the T_e and n_e profiles in figure 6. Agreement with p_{div}^{expt} = 25 ± 3 mTorr is significantly improved compared to the previous neutral modeling studies for the C-Mod divertor [10,12]. The absolute error in the calculated pressure is representative of uncertainties in the neutral collision models in EIRENE.

Figure 7a plots the source strengths for the listed divertor regions (the divertor is defined as the vertical target region below a line connecting the inner and outer "noses"). The total volume recombination source, S_{rec}, is 1.7×10^{22} s^{-1}, which is on the same order as values from direct analysis of the $T_{e,Saha}$ and $n_{e,Stark}$ data [2] and 40% more than the total ion target

flux of 1.2×10^{22} s^{-1}. Note that the *effective* volume recombination source is presented here; see section 3.1.

The contribution of each neutral source to p_{div}^{code} is shown in figure 7b. The outer PFZ target flux produces nearly half of the divertor pressure due to its close proximity to the plenum entrance, and despite having only ~⅓ the source strength of volume recombination in the PFZ. Almost all of the neutrals produced in the SOL are pumped by the plasma before entering the plenum.

The dependence of p_{div}^{code} on individual neutral processes is determined by removing each process in turn and recalculating the pressure; see figure 8. The neutral solution is most sensitive to Ly_α trapping, viscosity, and elastic collisions between plasma ions and neutral molecules, which are discussed in sections 3.1 to 3.3.

It is important to acknowledge that the above results are for a "sealed plenum" approximation where the *only* neutral leakage pathway between the plenum and the main chamber is through the divertor throat (the same assumption was made in the previous studies divertor studies [10,12]). The decrease in p_{div}^{code} after including a more realistic representation of the outer divertor structure in the model is discussed in section 3.4.

3.1 Volume recombination and opacity to Ly_α photons

Radiative, 3-body and molecular assisted recombination [20] (MAR) contribute 1%, 89%, and 10% of the total recombination source, respectively.

The peak atom density in the PFZ is 1.3×10^{20} m^{-3}, and the associated absorption of Ly_α photons can result in a significant steady-state population of excited $n_D(p=2)$ atoms. The ionization potential is lower for the excited atoms (3.4 eV) than for the ground state (13.6 eV),

which substantially increases the ionization rate in regions of low T_e, i.e. the PFZ. The loss of the photon from the system when the absorber is ionized before re-emission is referred to as "trapping".

If photon transport is *not* included in the neutral model, the calculated divertor pressure increases to ~25 mTorr. For photon transport included, ~90% of the Ly_α photons emitted in the PFZ are trapped, consistent with strong trapping levels observed experimentally [2]. The prompt re-ionisation of atoms due to Ly_α opacity effectively reduces S_{rec} in the PFZ by a factor ~2. The model employed here includes Doppler and natural broadening, and follows Ly_α photons only. Zeeman splitting (in development) will reduce the trapping but this will be offset by the inclusion of additional Lyman lines.

3.2 Neutral viscosity

The neutral molecule density, n_{D_2}, is plotted in figure 9a. The density gradient at the entrance to the plenum is due to: (a) the temperature gradient between higher energy molecules outside the plenum, which have partially thermalized with the plasma via D^+–D_2 elastic collisions, and the colder gas inside the plenum that has thermalized with the walls, and (b) the higher energy neutrals "pushing" on the colder plenum gas via neutral-neutral collisions. The difference between the radial variation in n_{D_2} through the plenum entrance (white dashed line in figure 9a) for the viscous and inviscid neutral solutions is shown in figure 9c.

Figure 9b shows the neutral molecule pressure, p_{D_2}. The molecular pressure is 25 mTorr just outside the plenum, but roughly half of the neutral momentum is lost to the wall

near the entrance, giving a lower pressure inside the plenum. The radial variation in p_{D_2} is shown in figure 9d for cases with and without viscosity.

Neutral-plasma interactions dominate outside the plenum and therefore the solution in the divertor proper is not strongly affected by neutral viscosity, unlike in the plenum.

3.3 D^+ –D_2 elastic collisions

Removing elastic collisions between plasma ions and neutral molecules reduces the divertor pressure by a factor 3–4 to 5 mTorr. This strong dependence is a result of the high probability that molecules exiting the plenum will scatter off the cold, dense plasma in the outer PFZ. This is referred to as the *albedo*, A, of the plasma. For a given "primary influx" of neutrals into the plenum (particles entering for the first time), Φ_0, the total influx, Φ_{tot}, consists of Φ_0 plus the flux of neutrals that exit and then return before they are ionized by the plasma. Φ_{tot} (Φ_0, A) is given by:

$$\Phi_{tot} = \frac{\Phi_0}{1 - A}, \qquad (1)$$

which is highly nonlinear as A $\rightarrow$ 1. For the plasma solution in section 2.3, A is 0.81 when D^+–D_2 elastic collisions are included and Φ_{tot} is a factor 5 higher than Φ_0. Removing D^+–D_2 gives A = 0.55, with A non-zero because neutrals can still return to the plenum after wall collisions or dissociation.

This strong dependence of Φ_{tot} on the D^+–D_2 collision rate for A $\rightarrow$ 1 suggests that p_{div}^{code} is sensitive to $\sigma_{D^+-D_2}$, and indeed, increasing $\sigma_{D^+-D_2}$ by 50% in the model raises the pressure to 21 mTorr. However, the cross-sections in EIRENE are in agreement with recent quantal calculations [21] with uncertainties less than 50%.

3.4 Divertor leakage

There are toroidal and poloidal gaps in the C-Mod outer divertor which provide additional leakage pathways for neutrals to escape the plenum. Including these pathways in the model via a 3D representation of the outer divertor in EIRENE [10] reduces p_{div}^{code} to 11 ± 3 mTorr, significantly increasing the discrepancy with the measured pressure. Note that much of the above analysis is still valid since p_{div}^{code} is only lower by 40%, but the 3D result suggests that an important aspect(s) of the C-Mod divertor is still not included in the model.

4. Summary and conclusions

The calculated divertor pressure for 3D EIRENE, which includes all significant leakage pathways from the plenum to the main chamber, was 11 ± 3 mTorr, a factor ~2 lower than the measured pressure of 25 ± 3 mTorr. The result for the "sealed plenum" approximation is 17 ± 2 mTorr, a factor 5–6 higher than for the previous neutral modeling studies of the C-Mod divertor. The neutral solution was strongly influence by opacity to Ly_α photons, viscosity, and elastic collisions between plasma ions and neutral molecules. Note that the pressures reported here are the first C-Mod results to include the effect of Ly_α trapping, which *reduces* the calculated pressure by ~30%.

The reduction in the discrepancy with experiment was due to more detailed modeling of detached plasma profiles, in particular the introduction of partially detached plasma in the outer PFZ. The empirical plasma model successfully generated a divertor plasma solution that has broad agreement with the available experimental data, within uncertainties.

Exceptions were the magnitude of the D_α and D_γ emissions which where high in the model by a factor ~2.

The results indicate that much of the controlling neutral physics for a collisional, "ITER-like" divertor is well represented in EIRENE. Future work to investigate the remaining factor ~2 discrepancy with the measured pressure includes a continuing review of the experimental data, refinement of the plasma solution, more complete opacity modeling, an approximation for plasma oscillations, better characterization of the lower divertor (more data), the inclusion of additional charge carriers (H_2^+, H_3^+, H^-) near surfaces in the lower divertor, and the transport of vibrationally excited molecules into the plenum.

5. Acknowledgements

This work was supported by US DOE Contract No. DE-AC02-78ET51013 and the National Sciences and Research Council of Canada.

References

[1] G. M. McCracken, *et al.*, J. Nucl. Mater. **266-269** (1999) 37
[2] B. Lipschultz, *et al.*, Phys. Plasmas **6** (5) (1999) 1907
[3] A. S. Kukushkin, *et al.*, Nucl. Fus. **42** (2002) 187
[4] D. B. Heifitz, *Physics of Plasma Wall Interaction in Controlled Fusions*, Oxfort:Plenum Press, 1986, p 695.
[5] J.L. Terry, *et al*., Phys. Plasmas **5** (5) (1998) 1759
[6] Reiter D, *The EIRENE Code,* http://www.eirene.de/
[7] D. P. Stotler, C. F. F. Karney, Contrib. Plasma Phys. **34** (1994) 392
[8] I. H. Hutchinson, *et al.*, Phys. Plasmas **1** (5) (1994) 1511
[9] A. Niemczewski, *et al.*, Nucl. Fusion **37** (2) (1997) 151
[10] D. P. Stotler, *et al.*, J. Nucl. Mater. **290-293** (2001) 967
[11] J. D. Elder, *et al.* 2000 APS poster, http://starfire.utias.utoronto.ca/DIVIMP/publications/
[12] D. P. Stotler, *et al.*, PPPL Report 3690 (2002)
[13] S. Lisgo, Ph.D. thesis, http://starfire.utias.utoronto.ca/DIVIMP/publications/
[14] D. E. Post J. Nucl. Mater. **220-222** (1995) 143
[15] P.C. Stangeby, *The Plasma Boundary of Magnetic Fusion Devices*, Institute of Physics Publishing, Bristol (2002).
[16] S. Lisgo, P. C. Stangeby, *et al.*, *these proceedings*
[17] B. LaBombard, *et al.*, J. Nucl. Mater. **220-222** (1995) 976
[18] G. Fussmann, *et al.*, J. Nucl. Mater. **128-129** (1984) 350
[19] E. M. Hollmann, *et al.*, Rev. Sci. Instrum. **74** (9) (2003) 3984
[20] U. Fantz, *et al.*, J. Nucl. Mater. **290-293** (2001) 367
[21] P. S. Krstic and D. R. Schultz**,** *Atomic and Plasma Material-Interaction Data for Fusion*, Volume 8, Vienna: IAEA, 1998

Table Caption

Table 1: Estimate of divertor collisionality. n_e is the electron density in the divertor and R is the major radius.

Figure Captions

Figure 1: Poloidal cross-section of the C-Mod divertor showing the available diagnostics: (1) target Langmuir probe arrays, (2) vertical reciprocating probe, (3) top-view photodiode array (D_α, shaded), (4) side-view photodiode array (D_α, shaded), (5) top-view spectrometer chords, (6) side-view spectrometer chords, (7) inversion region for a toroidally viewing CCD camera, and (8) pressure gauge.

Figure 2: (a) – (d) Target Langmuir probe data (solid squares) compared to plasma model boundary conditions (lines). In (a), spectroscopic near-target T_e data is included (open squares). (e) Outer target (solid), inner target (dashed) and upstream plasma pressure (dotted, from reciprocating probe).

Figure 3: Top-view spectroscopic data. See text for notes.

Figure 4: Side-view spectroscopic data.

Figure 5: Comparison of (a) experimental and (b) code D_γ profiles.

Figure 6: Divertor plasma solution input to EIRENE.

Figure 7: (a) Neutral source strengths for thee divertor. (b) The percentage of the calculated neutral pressure generated by neutrals from the individual sources.

Figure 8: The change in the calculated neutral pressure when various processes are removed from the neutral model in EIRENE.

Figure 9: (a) The neutral molecule density distribution for the standard case. (b) The neutral molecule pressure for the standard case. (c) Radial variation [along the dashed horizontal line in (a)] of the molecule density with (solid) and without (dashed) viscosity included in the model. (d) Radial pressure variation, as in (c).

Tokamak	R (m)	n_e (10^{20} m^{-3})	n_e R
JET [1]	2	2.9	6
C-Mod [2]	0.68	15	10
ITER [3]	6.2	10	62

Table 1

Figures

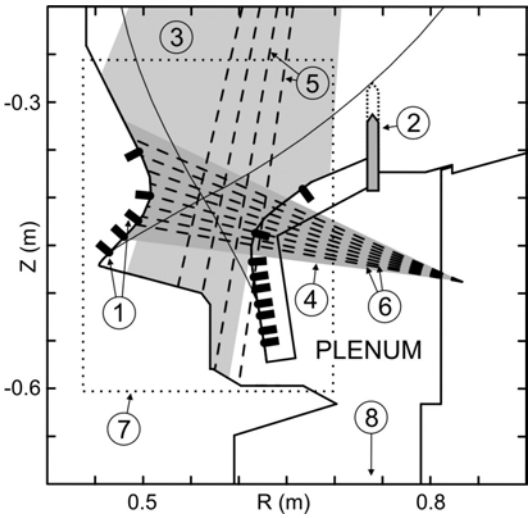

Figure 1

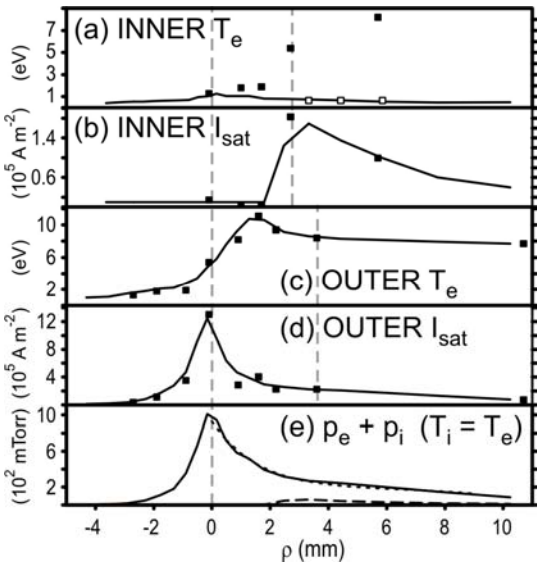
(a) INNER T_e
(eV)
(b) INNER I_{sat}
(10^5 A m^{-2})
(c) OUTER T_e
(eV)
(d) OUTER I_{sat}
(10^5 A m^{-2})
(e) $p_e + p_i$ ($T_i = T_e$)
(10^2 mTorr)
ρ (mm)

Figure 2

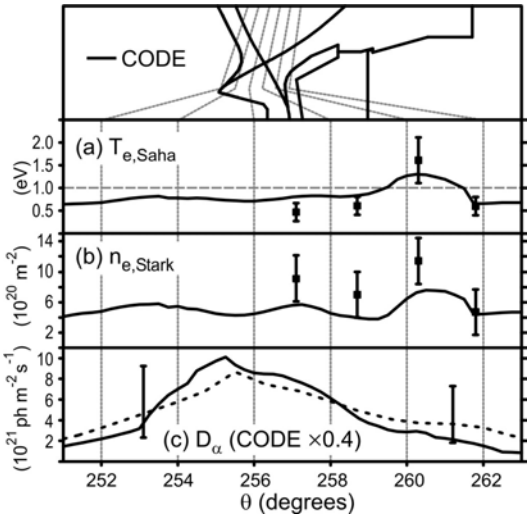
CODE
(a) $T_{e,Saha}$
(eV)
2.0
1.5
1.0
0.5
(b) $n_{e,Stark}$
$(10^{20}\ m^{-2})$
14
10
6
2
$(10^{21}\ ph\ m^{-2}\ s^{-1})$
10
8
6
4
2
(c) D_α (CODE ×0.4)
252
254
256
258
260
262
θ (degrees)

Figure 3

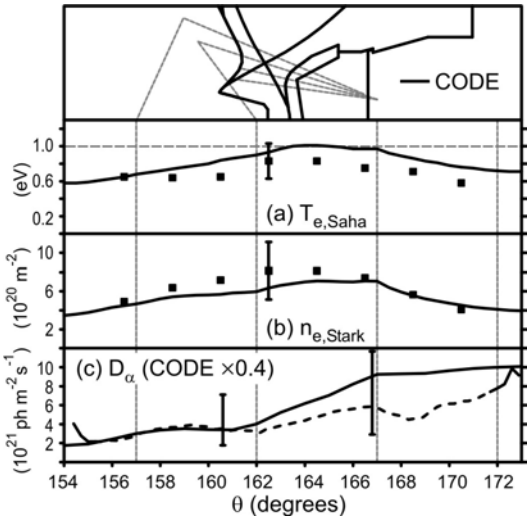
CODE
(eV)
1.0
0.6
0.2
(a) $T_{e,Saha}$
$(10^{20}\ m^{-2})$
10
6
2
(b) $n_{e,Stark}$
$(10^{21}\ ph\ m^{-2}\ s^{-1})$
(c) D_α (CODE ×0.4)
10
8
6
4
2
154 156 158 160 162 164 166 168 170 172
θ (degrees)

Figure 4

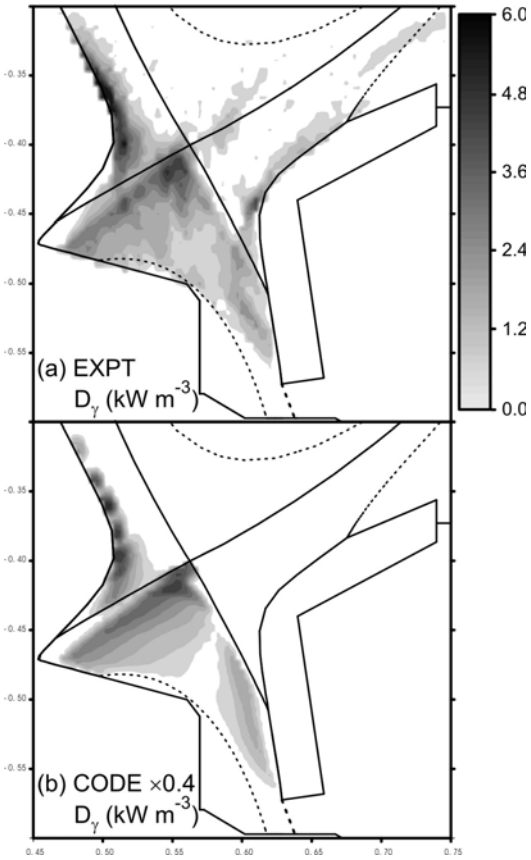

Figure 5

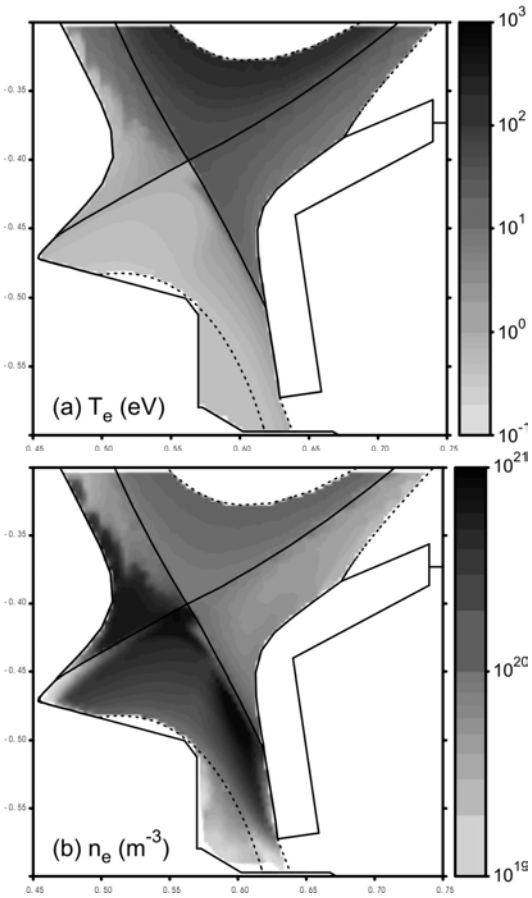

Figure 6

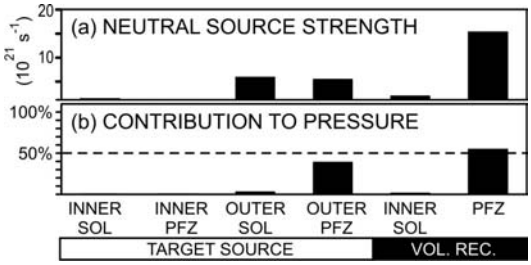
(a) NEUTRAL SOURCE STRENGTH
20
10
$(10^{21}\ s^{-1})$
(b) CONTRIBUTION TO PRESSURE
100%
50%
INNER SOL
INNER PFZ
OUTER SOL
OUTER PFZ
INNER SOL
PFZ
TARGET SOURCE
VOL. REC.

Figure 7

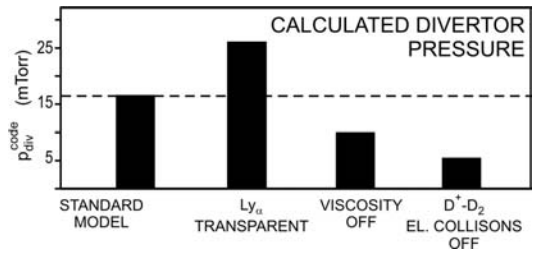
CALCULATED DIVERTOR PRESSURE
25
15
5
(mTorr)
p_{div}^{code}
STANDARD MODEL
Ly_α TRANSPARENT
VISCOSITY OFF
D^+-D_2 EL. COLLISONS OFF

Figure 8

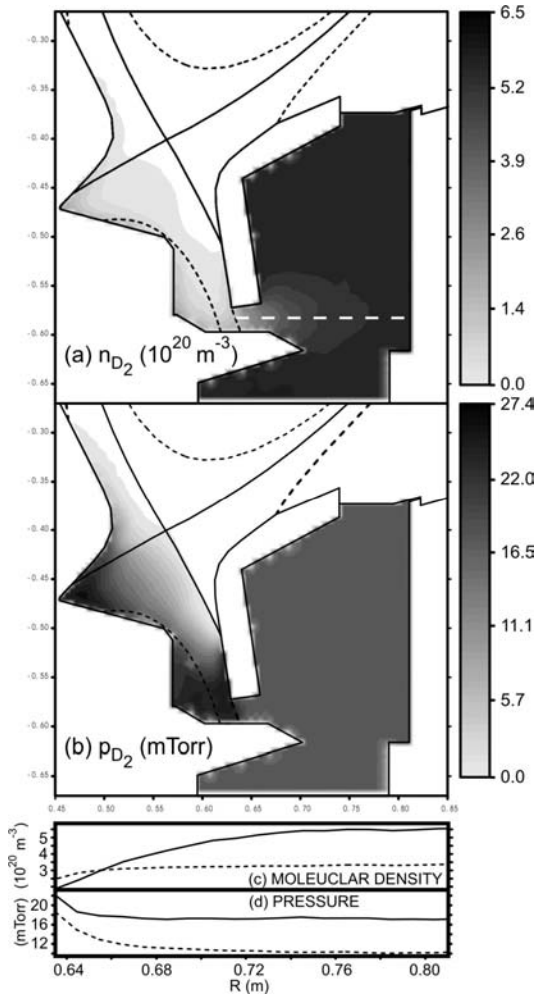
(a) n_{D_2} (10^{20} m^{-3})
6.5
5.2
3.9
2.6
1.4
0.0
(b) p_{D_2} (mTorr)
27.4
22.0
16.5
11.1
5.7
0.0
(c) MOLEUCLAR DENSITY
(d) PRESSURE
(10^{20} m^{-3})
(mTorr)
R (m)
0.64
0.68
0.72
0.76
0.80

Figure 9